Geophysical Research Letters

RESEARCH LETTER
10.1029/2022GL100970

Experimental Constraints on the Rheology of Lavas From 2021 Cumbre Vieja Eruption (La Palma, Spain)

F. Di Fiore[1], A. Vona[1], A. Scarani[1], G. Giordano[1,2], C. Romano[1], D. Giordano[3,4], L. Caricchi[5], A. Martin Lorenzo[6,7], F. Rodriguez[6], B. Coldwell[6,7], P. Hernandez[6,7], and M. Pankhurst[6,7]

[1]Dipartimento di Scienze, Università degli Studi Roma Tre, Roma, Italy, [2]Istituto di Geologia Ambientale e Geoingegneria - Consiglio Nazionale delle Ricerche, Roma, Italy, [3]Earth Sciences Department, University of Torino, Torino, Italy, [4]Centro Nazionale delle Ricerche, Istituto di Geoscienze e Georisorse, Pisa, Italy, [5]Department of Earth Sciences, University of Geneva, Geneva, Switzerland, [6]Instituto Volcanológico de Canarias (INVOLCAN), La Laguna, Spain, [7]Instituto Tecnológico y de Energías Renovables (ITER), Granadilla de Abona, Spain

Key Points:

- High-*T* deformation experiments characterize the rheology of Cumbre Vieja lavas under both disequilibrium and equilibrium conditions
- Two different rheological responses are observed in relation to the increased disequilibrium conditions at which the melt is subjected
- Integration of experimental and field data permits to understand the mechanisms that enhance the flowing ability of these lavas

Supporting Information:

Supporting Information may be found in the online version of this article.

Correspondence to:

F. Di Fiore and A. Vona,
fabrizio.difiore@uniroma3.it;
alessandro.vona@uniroma3.it

Citation:

Di Fiore, F., Vona, A., Scarani, A., Giordano, G., Romano, C., Giordano, D., et al. (2023). Experimental constraints on the rheology of lavas from 2021 Cumbre Vieja eruption (La Palma, Spain). *Geophysical Research Letters*, *50*, e2022GL100970. https://doi.org/10.1029/2022GL100970

Received 23 AUG 2022
Accepted 27 JAN 2023

Author Contributions:

Conceptualization: F. Di Fiore, A. Vona
Data curation: F. Di Fiore
Funding acquisition: A. Vona, G. Giordano, C. Romano
Investigation: F. Di Fiore, A. Scarani
Methodology: F. Di Fiore
Project Administration: G. Giordano, M. Pankhurst

Abstract The 2021 Tajogaite eruption of Cumbre Vieja (La Palma, Spain) was typified by the emission of low viscosity lavas that flowed at high velocities and inundated a large area. We experimentally investigated the rheological evolution of melt feeding the eruption through concentric cylinder viscometry to understand the exceptional flowing ability of these lavas and constrain its emplacement dynamics. We conducted a set of cooling deformation experiments at different cooling rates (from 0.1 to 10 °C/min), and isothermal deformation experiments at *subliquidus* dwell temperatures between 1225 and 1175°C. All experiments were conducted at a shear rate of 10 s^{-1}. Results show that disequilibrium crystallization and its timescale fundamentally control the rheological evolution of the melt, resulting in different rheological response to deformation of the crystal-bearing magmatic suspension. Integrating rheological data with field observations allows us to shed light on the mechanisms that govern the high flowability of these lavas.

Plain Language Summary Understanding and modeling the mechanisms controlling the inundation ability of lava flows is pivotal for hazard assessment and mitigation of related risk. Lavas flowing across the Earth's surface experience different cooling conditions. These conditions are related to the thermal gradients generated at various levels within the flow's thickness. Especially for extremely fluid magmas such as those erupted at Cumbre Vieja, the different cooling paths (and different disequilibrium conditions) that lava flows experience strongly influence the crystallization processes. Both cooling and crystallization produce an increase of lava viscosity, hindering lava flowability. If crystallization occurs over timescales shorter than those of cooling, the presence of crystals may give rise to more complex flow behavior and emplacement style, including flow rupture and separation. Such conditions may favor the development of flow decoupling and lava tunnel formation. In this study we experimentally investigate the viscosity evolution of the Tajogaite lavas and the transition from pure viscous flow to more complex responses to deformation. Then, we use our data set in concert with field observation to constrain the dynamics governing the emplacement style of these lavas.

1. Introduction

1.1. The 2021 Tajogaite Eruption

La Palma is an active volcanic island of the Canary archipelago (Spain). The Holocene to historical activity has erupted mostly mafic magmas (basanite to tephrite), from monogenetic effusive to mild explosive centers forming the Cumbre Vieja ridge. After 50 years of quiescence, on 19 September 2021 a new violent strombolian and effusive eruption started on the western slope. The eruption lasted ~3 months until 13 December, emplacing about 0.2 km^3 of lava and tephra (Civico et al., 2022), inundating ~12.5 km^2 of land, covering more than 100 km^2 by variable thickness of scoria lapilli and ash, severely affecting the local communities (Oterino et al., 2021). Magma composition spans the tephrite-basanite fields, and the lavas are texturally porphyritic with clinopyroxene ± amphibole ± titanomagnetite ± olivine showing mean crystal contents of ~18-4-2-2%, respectively (Pankhurst et al., 2022). While the violent strombolian activity fed by several vents aligned along a NW-trend built a ~200 m high scoria cone, the lava issued almost continuously (González, 2022). The average mass eruption rate was 27 m^3/s and lava temperature of 1140°C (Carracedo et al., 2022). The resulting lava flows initiated as open channels with smooth upper surfaces that transitioned laterally to brecciated 'a'ā top along the

Resources: A. Vona, G. Giordano, C. Romano, L. Caricchi, A. Martin Lorenzo, F. Rodriguez, B. Coldwell, P. Hernandez, M. Pankhurst
Supervision: A. Vona, G. Giordano, C. Romano, M. Pankhurst
Visualization: F. Di Fiore, A. Vona, D. Giordano, L. Caricchi
Writing – original draft: F. Di Fiore
Writing – review & editing: A. Vona, A. Scarani, G. Giordano, C. Romano, D. Giordano, L. Caricchi, A. Martin Lorenzo, F. Rodriguez, B. Coldwell, P. Hernandez, M. Pankhurst

steep upper slopes (up to 20°). Several tubes formed along the lowest inclined section of the island (~5°). Breakout events progressively expanded the lava field to its final extension (Figure S1 in Supporting Information S1).

1.2. Rheology of Low-Viscosity Lavas

The lavas erupted during the 2021 Cumbre Vieja eruption show a high flowing ability due to the low-viscosity typical of mafic and alkaline melts (Campagnola et al., 2016; Chevrel et al., 2015; Di Fiore, Vona, et al., 2021; Di Fiore, et al., 2022; Giordano & Dingwell, 2003; Ishibashi, 2009; Ishibashi & Sato, 2007; Jones et al., 2022; Kolzenburg, Di Genova, et al., 2018; Kolzenburg et al., 2016; Kurokawa et al., 2022; Sato, 2005; Sehlke et al., 2014; Vetere et al., 2019; Vona et al., 2011, 2017). Low viscosity also facilitates efficient degassing (Namiki et al., 2022) and promotes fast crystallization kinetics due to rapid chemical diffusion (Mollo & Hammer, 2017). Consequently, lava solidification paths and emplacement styles are primarily controlled by the crystallization efficiency, which in turn is strongly influenced by the cooling conditions that a flow experiences (Arzilli et al., 2022; Di Fiore, Vona, et al., 2021; Di Fiore, et al., 2022; Giordano et al., 2007; Kolzenburg et al., 2016, 2020). Therefore, understanding magma rheological behavior across different cooling paths is essential to understand the high flowing ability of these lavas.

Here we present results from a suite of concentric cylinder experiments designed to characterize the high-*T* *subliquidus* rheology of the 2021 Cumbre Vieja lavas under both disequilibrium and near-equilibrium conditions. A set of Cooling Deformation Experiments (CDE) was carried out to explore the crystallization kinetics and the related rheological behavior at constant cooling conditions pertinent to lava flow emplacement (Di Fiore, Vona, et al., 2021; Di Fiore, et al., 2022; Giordano et al., 2007; Kolzenburg, Di Genova, et al., 2018; Kolzenburg et al., 2020, 2022). To mimic the high-deformation regime at which the flow was subjected (i.e., high-*T* emplacement, low-viscosity, steep slopes; see Section 1.1) we adopted a fixed shear rate of 10 s^{-1}. In addition, a set of Isothermal Deformation Experiments (IDE) was conducted at constant *subliquidus* temperatures to characterize the effect of near-equilibrium crystal contents and textures on melt viscosity (Campagnola et al., 2016; Chevrel et al., 2015; Di Fiore, Mollo, et al., 2021; Di Fiore, Vona, et al., 2021; Ishibashi, 2009; Sehlke et al., 2014; Vona et al., 2011). This integrated approach permits to describe the rheological evolution of the Tajogaite lavas and analyze the emplacement dynamics of these extraordinarily mobile lava flows.

2. Materials and Methods

2.1. Starting Material and Sample Preparation

The lava samples used for our study are basanitic in chemical composition (Pankhurst et al., 2022; Table S1 in Supporting Information S1) and were collected during a field campaign in October 2021 (Figure S1 in Supporting Information S1 for sampling location). Rock samples were powdered using a jaw crusher and a ring-mill and then melted in a Pt crucible in a Nabertherm® $MOSi_2$ box furnace at 1400°C, air oxygen fugacity and atmospheric pressure.

2.2. Crystal-Free Melt Viscosity

Crystal-free melt viscosity (η_{liquid}) data were obtained through high-*T* *superliquidus* measurements in a Concentric Cylinder apparatus (CC) and from calorimetric measurements at *T* close to the glass transition temperature (Tg) using a Differential Scanning Calorimeter (DSC).

For high-*T*, CC viscometry was conducted with a Rheotronic II Rotational Viscometer (Theta Instruments) installed at the EVPLab of the University of Roma Tre. The apparatus is equipped with an Anton Paar Rheolab Qc viscometer head with a full-scale of torque of 75 mNm (see Supplementary Methods Section S1 in Supporting Information S1 for calibration procedure details). The glassy materials were loaded into Pt80Rh20 cylindric crucibles (62 mm in height, with a 32 mm inner diameter) and stirred at $\dot{\gamma}$ of 10 s^{-1} with a Pt80Rh20 spindle (3.2 and 42 mm in diameter and length, respectively) at 1400°C and ambient pressure for 3 hr to ensure chemical and thermal homogenization. Then the furnace temperature was progressively lowered to the following target temperatures: 1350-1301-1276-1250°C. At each temperature, η_{liquid} values were collected after the attainment of steady torque and temperature values (~45 min).

For low-*T*, η_{liquid} was estimated through sets of DSC measurements on quenched crystal-free glasses (absence of nanolite was verified through Raman analyses) from CC, and the adoption of a parallel shift factor that we used to

convert calorimetric traces across the glass transition interval into melt viscosity values (Gottsmann et al., 2002; Di Genova et al., 2020; Scarani, Vona, et al., 2022; Scarani, Zandonà, et al., 2022). We used a Netzsch Pegasus 404 DSC to measure the glass transition of samples at matching cooling and heating rates of 10 and 20°C/min in Ar-atmosphere. The temperature at the onset (T_{onset}) and peak (T_{peak}) of heat flow curves across the glass transition interval were transposed into melt viscosity using the parallel shift factors of $K_{onset} = 11.20$ and $K_{peak} = 9.84$ (Di Genova et al., 2020; Stevenson et al., 1995). Details of the technique are summarized in the Supplementary Methods Section S2 in Supporting Information S1.

The liquid viscosity curve (η_{liquid}) that expresses the T-dependence of the pure liquid viscosity data was obtained by fitting the above-mentioned data (Table S2 in Supporting Information S1) via the Vogel-Fulcher-Tammann (VFT) expression (Log $\eta_{liquid} = A + [B/(T - C)]$; Figure S2 in Supporting Information S1).

2.3. Crystal Bearing Melt Measurements

The *subliquidus* rheological characterization was carried out using the same CC apparatus. The *superliquidus* treatment was performed by stirring the melt at 1400°C, air oxygen fugacity and ambient pressure for ~2 hr at $\dot{\gamma}$ of 10 s^{-1}.

A set of Cooling Deformation Experiments (CDE) (Figure S3 in Supporting Information S1) was conducted with a fixed shear rate ($\dot{\gamma}$) of 10 s^{-1} and variable cooling rate (q) from 0.1 to 10°C/min. During cooling, a departure of apparent viscosity (η_a; i.e., the ratio between the shear stress and shear rate applied) from the VFT trend viscosity of Log 0.05 (Pa s) followed by a constant positive increase of η_a was adopted as proxy for the onset of crystallization (Figure S3 in Supporting Information S1). The temperatures and times at which these rheological departures from the VFT trend were observed during CDE were defined as T_{onset} and t_{onset}, respectively.

The experiments were interrupted (Figure S3 in Supporting Information S1) when the stress limit of the device (~10^5 Pa) was reached, approaching the "rheological cut-off" (Giordano et al., 2007), or when the measurements showed a stress drop indicative of viscous rupture behavior (Di Fiore, Vona, et al., 2021). The viscous rupture occurs when crystal-crystal interaction (i.e., onset of clumping; Soule & Cashman, 2005) in the suspension leads to a major shear localization event (Di Fiore, Vona, et al., 2021) that reflect in a large final drop during the viscosity measurements (Figure S3 in Supporting Information S1). Due to extremely fast crystallization kinetics and high viscosity observed at the end of each cooling segment, no sampling of experiments and post-run analyses (i.e., crystal contents and distribution) could be conducted. This represents the main limitation of the technique (cf. Di Fiore et al., 2022; Giordano, 2019; Kolzenburg, Di Genova, et al., 2018; Kolzenburg, Giordano, et al., 2018; Kolzenburg et a., 2022). At the end of each CDE, the sample is re-heated to 1400°C and re-homogenized for the subsequent cooling cycle.

Isothermal Deformation Experiments (IDE) (Figure S3 in Supporting Information S1) were carried out at *subliquidus* temperatures of 1225-1200-1175°C, under constant $\dot{\gamma}$ of 10 s^{-1}. For each IDE, the melt was cooled from *superliquidus* T of 1400°C to the target temperature at q of 25°C/min. The experiments were quenched after the achievement of a time independent value of η_a (i.e., stable crystal content, Vona & Romano, 2013; Figure S3 in Supporting Information S1). In this case, the post-run products were drilled, mounted in epoxy, and polished for textural analyses.

3. Results

3.1. CDE Results

The evolution of apparent viscosity (η_a) under different cooling rates (q) is shown as a function of temperature (T) and time (t) in Figures 1a and 1b. At *superliquidus* conditions, the rheological evolution trend of the melt of CDEs follows the VFT model, although the viscosity signals are noisy in the interval 1400–1350°C, due to the low viscosity values of the basanitic melt approaching the lower resolution limit of the device (Table S1 in Supporting Information S1).

The temperature of the rheological departure (T_{onset}) decreases from 1236 to 1122°C (Figure 1a, Table S3 in Supporting Information S1) as q increases from 0.1 to 10°C/min. The timespan necessary to observe the rheological departure (t_{onset}) from the start of each experiment decreases from ~9.8×10^4 to ~1.7×10^3 s with increasing q from 0.1 to 10°C/min (Figure 1b, Table S3 in Supporting Information S1).

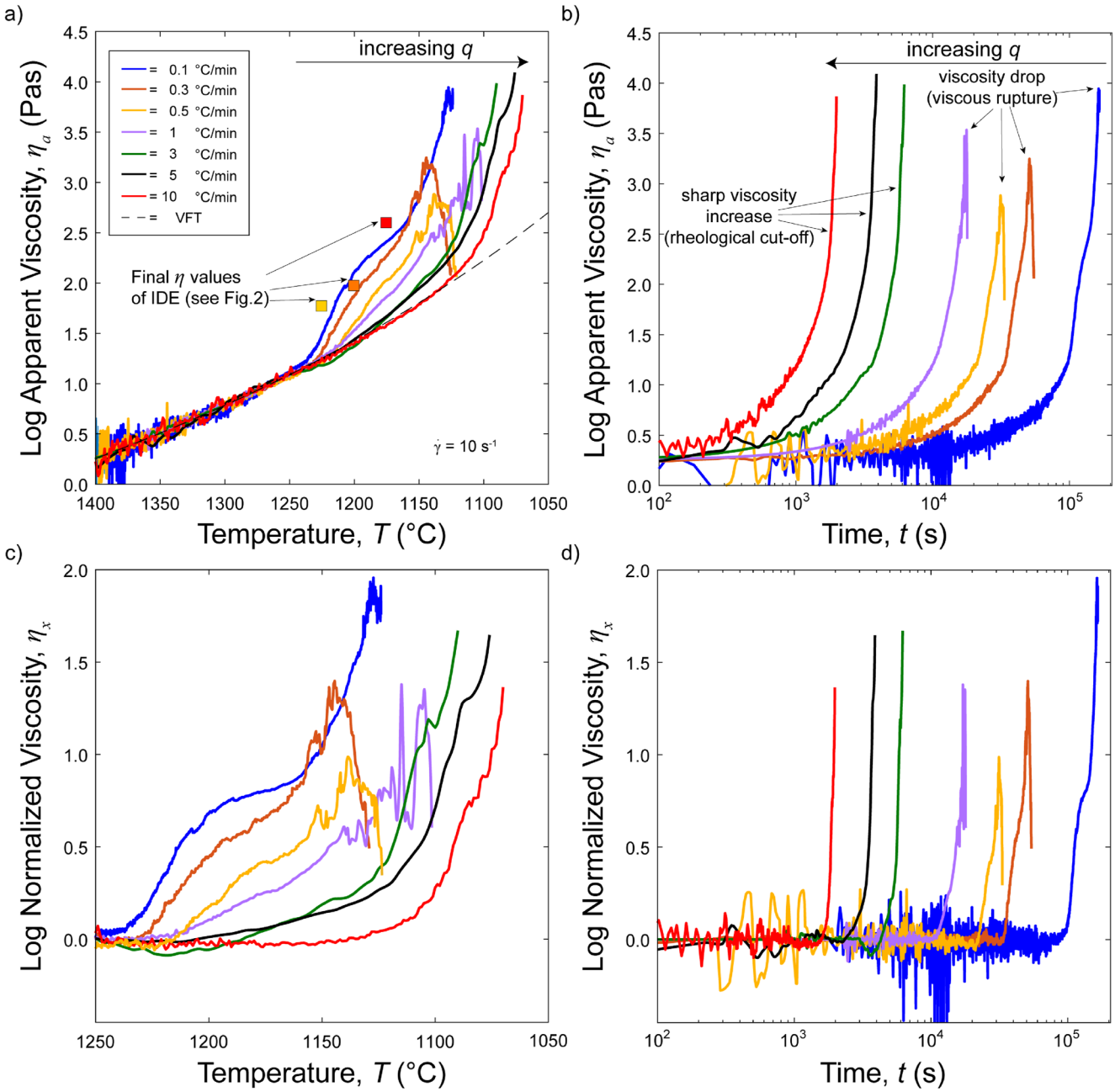

Figure 1. Summary of Cooling Deformation Experiments data. (a, b) Variation of apparent viscosity (η_a) as a function of experimental temperature (a) and time (b). In (a) the T-dependence of the pure liquid viscosity (VFT model; dashed line) and the results of the near-equilibrium crystallization experiments (IDE; squares) are also reported. (c, d) Variation of normalized viscosity (η_x) as a function of experimental temperature (c) and time (d).

After the onset of crystallization, two distinct trends of rheological evolution linked to the different degree of q applied are observed (i.e., from 0.1 to 1°C/min and from 3 to 10°C/min). In detail, the increase of viscosity in the experiments conducted at q of 0.1-0.3-0.5-1°C/min are characterized by a series of small viscosity drop. The experiments were interrupted when the viscous rupture was observed. The viscous rupture takes place at η_a ranging from Log 3.87 to 2.76 (Pa s), at temperatures (T_{vr}) spanning from 1135 to 1113°C, and times (t_{vr}) from ~1.62×10^5 to ~1.7×10^4 s (Figure 1, Table S3 in Supporting Information S1).

The experiments conducted at q of 3-5-10°C/min were interrupted when the stress limit of the device was reached at η_a Log ~4 (Pa s). These experiments are characterized by a sharp viscosity increase that leads to approach the rheological cut-off for this suspension. The cut-off temperatures ($T_{cut\text{-}off}$) and times ($t_{cut\text{-}off}$) decrease from 1090 to

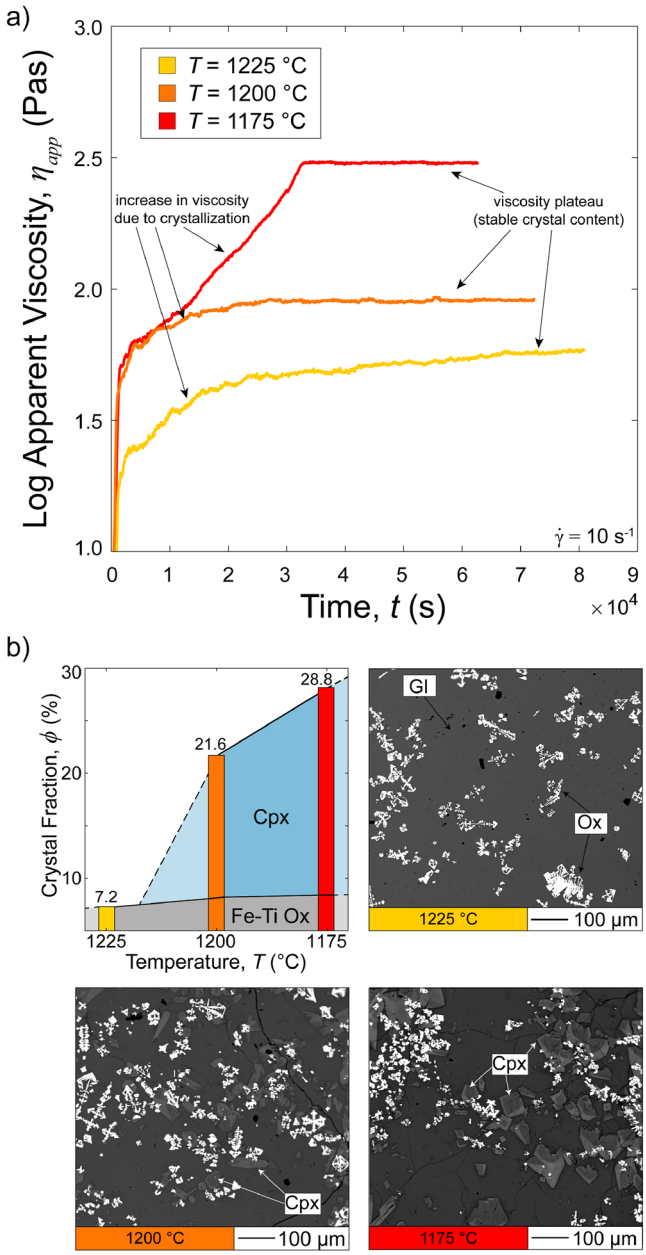

Figure 2. (a) Temporal evolution of Isothermal Deformation Experiments viscosity. (b) Diagram of crystal fraction variations at different dwell temperatures and representative BSE photomicrographs (50× magnification) of the post-run samples.

1070°C and from ~6.2×10^3 to ~2.0×10^3 s with increasing q, respectively (Figure 1, Table S3 in Supporting Information S1).

The effect of degree of crystallization on viscosity can be expressed by the normalized viscosity factor ($\eta_x = \eta_a/\eta_{liquid}$, Di Fiore et al., 2022). It should be noted that the normalized viscosity factor η_x is different from the relative viscosity parameter (η_r), the latter representing the ratio between the apparent viscosity and the viscosity of the suspending (residual) melt ($\eta_r = \eta_a/\eta_{res}$). The adoption of η_x results particularly useful in those cases such as that for the CDE technique which does not allow to discern and quantify the physical (i.e., presence of a solid phase) and chemical (i.e., suspending melt evolution) contributions of crystallization on the rheological evolution of the suspension. The maximum η_x values range from a minimum of 0.96 Log units for the run performed at q of 0.5°C/min to a maximum of 1.96 Log units at q of 0.1°C/min (Figure 1, Table S3 in Supporting Information S1).

3.2. IDE Results

The time-evolution of apparent viscosities (η_a) during IDE is shown in Figure 2a. The values measured at the steady state conditions increase from Log 1.77 to 2.48 (Pa s) (Table S3 in Supporting Information S1) with lowering the dwell T (from 1225 to 1175°C). The steady state conditions were achieved after t spanning from ~8.1×10^4 to ~6.3×10^4 s with decreasing dwell T.

Textural analysis of post-run products shows the ubiquitous presence of skeletal Fe-Ti oxides (Figure 2b). In the experiments conducted at 1200 and 1175°C clinopyroxene also appears, exhibiting a euhedral habit with hourglass texture (Figure 2b) or, often, showing complex intergrowth with the oxide crystals. Total crystal content increases from 7.2% to 28.8% (Figure 2b, Table S3 in Supporting Information S1) with decreasing temperature (from 1225 to 1175°C). Fe-Ti oxides show a slight increase in crystal fraction with decreasing dwell T (from 7.2% to 8.4%). Clinopyroxene is the most abundant phase in both the experiments in which is detected (i.e., 1200 and 1175°C, with a crystal fraction of 13.4% and 20.4%, respectively).

4. Discussion

4.1. Rheological Evolution of Tajogaite Basanitic Melt

The integration of rheological data obtained by different experimental approaches (i.e., IDE, CDE, and crystal-free melt viscosity) allows to delineate the thermo-rheological space in which crystallization takes place. The magnitude of crystallization, its timescales and influence on the rheological evolution of suspension are strictly linked to the degree of disequilibrium conditions that the melt experiences during cooling (Figure 3).

Using Figure 3a it is possible to qualitatively observe the viscosity-temperature window of this basanitic lava. The lower-η boundary corresponds to the minimum values of viscosity that a supercooled melt could achieve at both *superliquidus* and *subliquidus* temperatures and is defined by the crystal-free melt viscosity described by the VFT trend (Figure S2 in Supporting Information S1).

The upper-η boundary depicts the maximum viscosity values related to the maximum crystal contents attainable by the melt at a given temperature at equilibrium conditions. This boundary is qualitatively interpolated using the viscosity values (and related crystal contents) obtained through IDE (Chevrel et al., 2015; Di Fiore, Vona, et al., 2021; Vona et al., 2011). In the present case, the IDE display a progressive increment of the final η values

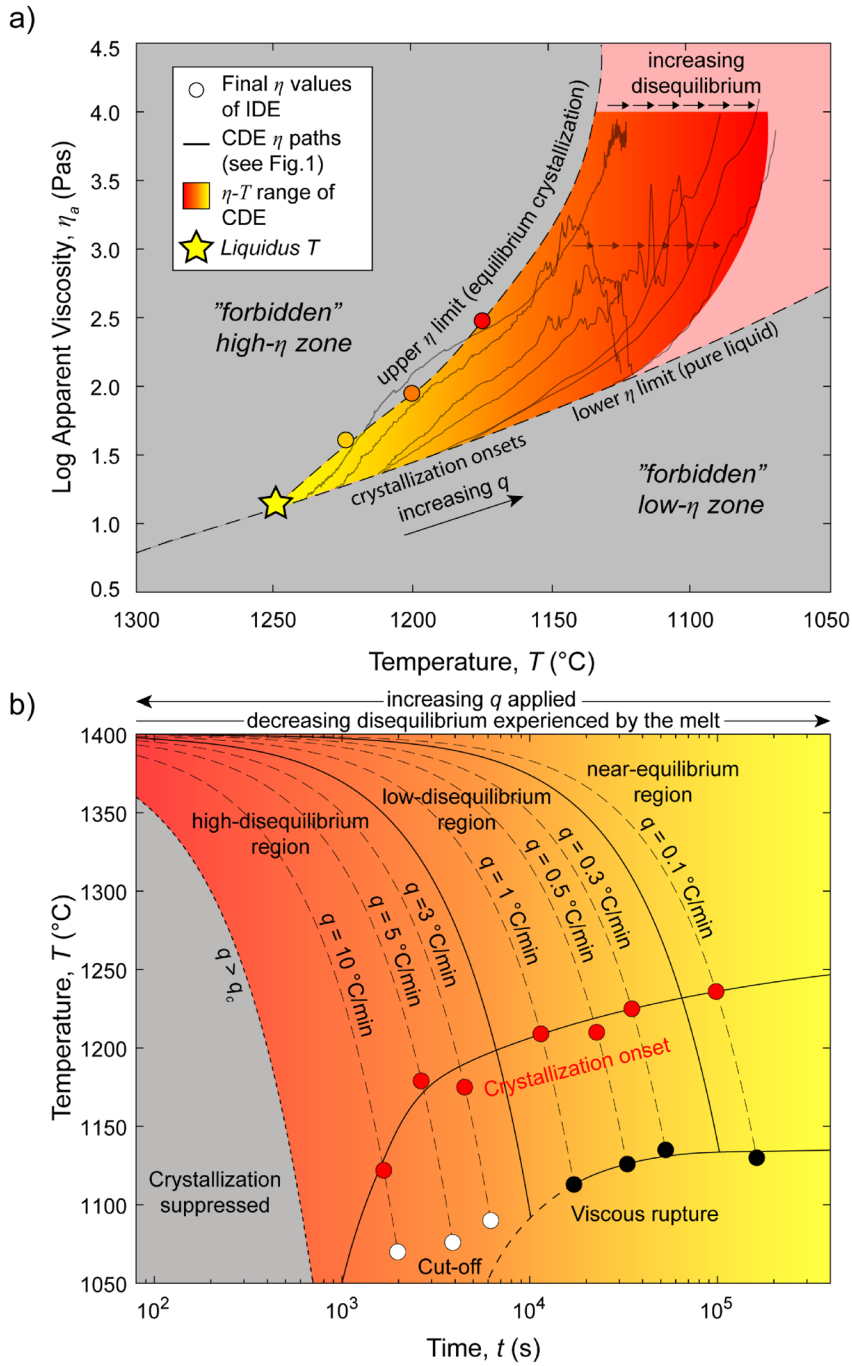

Figure 3. (a) Viscosity-temperature regime diagram for Tajogaite basanitic melt. (b) Time-temperature-transformation (TTT) diagram of the basanitic melt showing the effects of cooling rates on the crystallization process and rheological response of the suspension. Note that the critical cooling rate (q_c > 10°C/min) curve is only a qualitative guideline, not determined experimentally.

with decreasing dwell *T* due to the increased crystal fraction (Figure 2). The *liquidus T* of 1247°C calculated through the MELTS code (at air-oxygen fugacity conditions) results in excellent agreement with the equilibrium crystallization trend described by IDE.

Variable degrees of disequilibrium conditions characterize the crystallization of the melt within the thermo-rheological space depicted by the high-η and low-η boundaries (Figure 3a). CDE data explore such disequilibrium crystallization conditions typical for lava flow emplacement scenarios. In detail, with increasing

q both onset of crystallization and interruption of the experiment occur at progressively lower temperatures and the viscosity curves approach the lower-η boundary (maximum disequilibrium). Conversely, with decreasing q both rheological thresholds take place at higher temperatures and the viscosity paths track closer to the upper-η boundary, with CDE conducted at q of 0.1°C/min reaching final viscosities values comparable to those obtained by IDE. This indicates a progressive reduction of the degree of disequilibrium conditions at which the melt is subjected.

The different degrees of disequilibrium reflect different timescales of crystallization, spanning 2 orders of magnitude varying q (Table S3 in Supporting Information S1). In the *TTT*-diagram in Figure 3b, we identify three distinct zones linked to different timescales of crystallization and related to different q. These zones permit to delineate distinct regions of disequilibrium degrees that Tajogaite melt could have experienced as function of q. A "high-disequilibrium" region is identified for q from 3 to 10°C/min, in which the time interval of crystallization spans from $\sim 1.7 \times 10^3$ to $\sim 0.3 \times 10^3$ s (Table S3 in Supporting Information S1). A "low-disequilibrium" region, represented by q ranging from 0.3 to 1°C/min, is characterized by crystallization time that ranges from $\sim 1.8 \times 10^4$ to $\sim 5.8 \times 10^3$ s (Table S3 in Supporting Information S1). A third "near-equilibrium" region is defined by the run conducted at q of 0.1°C/min with the longest crystallization time of $\sim 6.4 \times 10^4$ s. The near-equilibrium conditions are confirmed observing Figure 1, in which the CDE run performed with the lowest q depicts the final viscosity values of IDE set.

In the CDE data set an intriguing behavior is represented by the onset of viscous rupture or the attainment of the rheological cut-off for the different runs. Primarily, viscous rupture only takes place for the measurements conducted with lower q (i.e., low-disequilibrium and near-equilibrium regions). In the experiments performed at higher q (i.e., high-disequilibrium region), viscous rupture did not occur within the experimental range investigated. In these experiments only a steep viscosity increase (rheological cut-off) of solidifying melt reaching the instrumental limit (i.e., Log $\sim$ 4 Pa s) was observed.

This behavior can be explained by the different timescales of crystallization across the experiment space. Although the CDE runs related to the high-disequilibrium region reach higher values of η, the interval of time in which the crystallization occurs is not sufficient to permit efficient development of particle-particle interaction (Di Fiore, Vona, et al., 2021; Soule & Cashman, 2005) and allow the solid fraction to create a continuous network. The latter, representing the preferential zone in which the shear localization develops, could facilitate the onset of viscous rupture. The high-disequilibrium conditions (i.e., CDE performed at $q > 1$°C/min) and the related short timespans hindered the formation of shear localization zone, shifting the onset of viscous rupture to lower temperatures and higher viscosity values, presumably outside of the measurable range of stress and viscosity of the CC apparatus. Similar behavior is observed in experiments conducted on a phonotephrite melt (Di Fiore, Vona, et al., 2021), in which viscous rupture took place at progressively higher viscosity values and lower temperatures with increasing the q applied.

4.2. Implications for Tajogaite Lava Flow Emplacement

The rheological measurements confirms that the low-η characterization of Tajogaite products is primarily responsible for the high-flood capacity of the erupted lavas. During the Tajogaite eruption lavas inundated an area of $\sim$12.5 km^2 in relatively short times (i.e. 19 September–13 December 2021; Longpré, 2021; Pankhurst et al., 2022).

In addition to the characteristic low-η, field observations showed that many mechanisms such as formation of channels and lava tubes (Figure 4a) played a key role on the flowing ability of these lavas. The development of lava tubes hinders heat dispersion that, in turn, affects the lava rheological evolution and its timescales, delaying nucleation and growth of crystals and promoting longer flows with respect to the open channels (Calvari & Pinkerton, 1999; Cashman et al., 1999, 2006).

Lava tube formation is commonly observed in pāhoehoe lavas and it is ascribed to different genetic processes (Kempe, 2019; Sauro et al., 2020). Field evidence indicate that most of the tubes at La Palma developed by lateral shelf accretion or "overcrusting" of channels (Sauro et al., 2020 and references therein). The latter process is led by rapid cooling of the upper lava flow surface in contact with air (Sauro et al., 2020). Fast cooling induces a rapid increase in viscosity until the solidification of the upper zone insulates the underlying flow and generate a rheological decoupling (Figure 4a). The insulation of the flow permits the maintenance of higher temperatures and low-η for longer times and, consequently, distances.

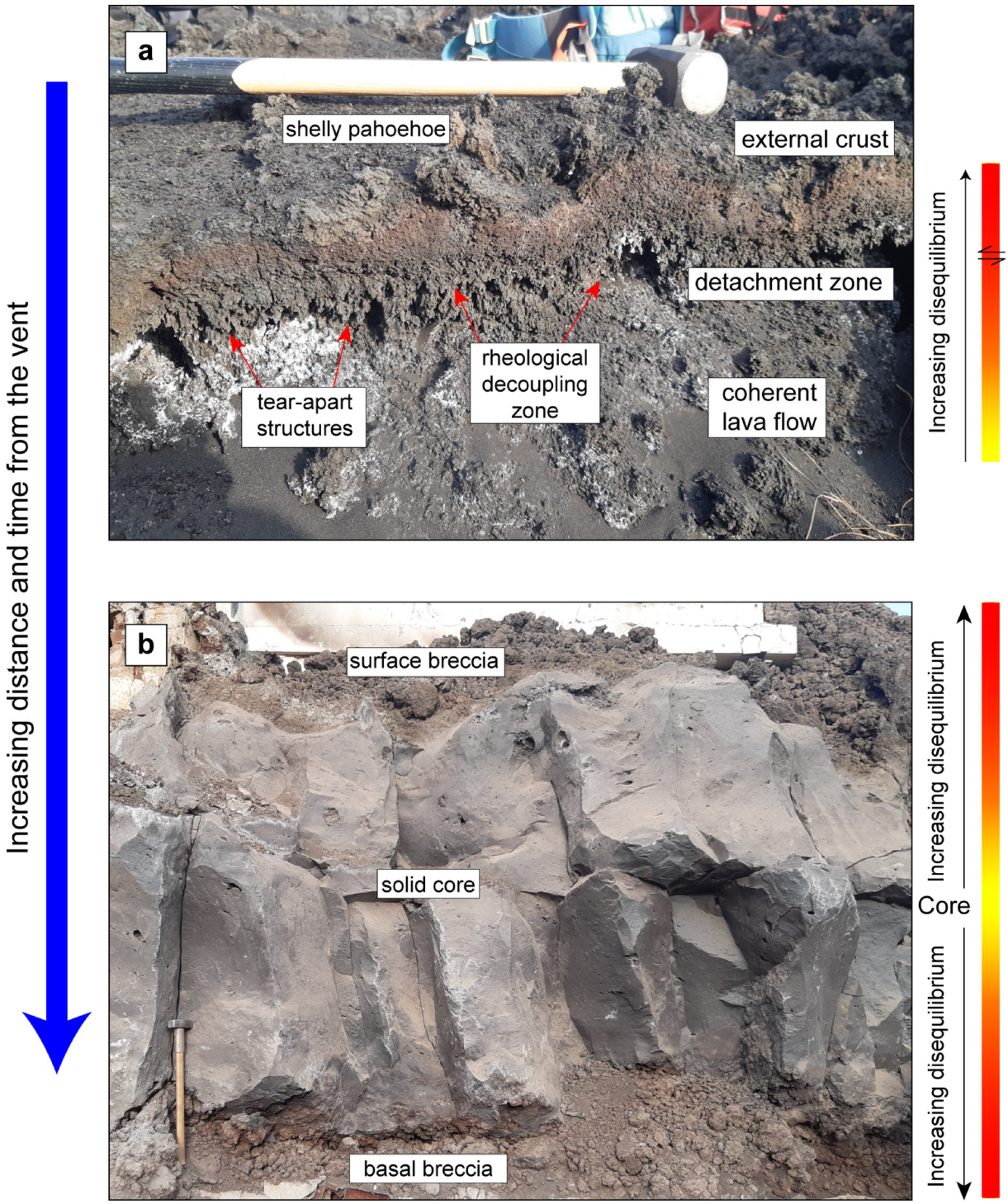

Figure 4. (a) Tear-apart structures on the upper crust of a lava flow outcropping near the vent. (b) Distal massive lava flow outcrop characterized by upper and basal breccias.

CDE data allow to map such rheological behavior driving the formation of lava tubes. The rheological data set presented in this study was obtained on a simplified system, being the experiments conducted under constant cooling and shear rates, at ambient pressure, air-oxygen fugacity, on degassed (i.e., bubble-free) and initially crystal-free melts. Even if natural lava flows as those emplaced during Tajogaite eruption are subjected to more complex dynamics (e.g., increased oxidizing conditions that could shift to lower *T* the crystallization onset

of Fe-Ti oxides phases; see Supplementary Discussion Section SD1 in Supporting Information S1), our data set permits to constrain the influence of a key parameter such as cooling rate on their rheological evolution.

The wide experimental range of q adopted in CDE reflects thermal gradients that a lava flow experiences at various heights along a vertical profile (Cashman et al., 1999; Harris & Rowland, 2009). In the most exterior part q values are the largest, producing the maximum disequilibrium conditions (Figure 3b). As illustrated by CDE experiments at $q > 3$°C/min, such circumstances promote fast solidification and a rapid increase of viscosity reaching the rheological cut-off at $t < 6{,}000$ s (Figures 1a and 1b) without major crystallization (Figures 1c and 1d). This mechanism leads to the formation of the upper crust of the lava flow (Figure 4a) that marks the evolution in lava tubes.

Subsequently, a detachment zone develops between the crust and the underlying lava (Figure 4a). The latter is subjected to progressively decreasing q (and disequilibrium conditions; Figure 3b) toward the core of the flow, due to the insulation produced by the external crust. Under these circumstances, analogous to those of CDE conducted at $q < 1$°C/min, the insulation allows the maintenance of high-T and low-η conditions for longer durations (Figure 1b). The result is a higher flowing ability of lava within the tunnel as observed in Tajogaite flows.

Notably, for longer timespans, experiments at $q < 1$°C/min also show the onset of viscous rupture. Such rheological thresholds occur at times (s) two orders of magnitude larger with respect to those necessary to reach the cut-off at faster q (Figures 1 and 3b). As discussed above, in this case the lower disequilibrium degree allows the development of a crystal-network that is the key factor responsible for the onset of rupture behavior. Importantly, the increase in lava viscosity and the attainment of the viscous rupture behavior is delayed, taking place further from the vent with the formation of autobreccia (Figure 4b) causing the pāhoehoe-ʻaʻā morphological transition (Cashman et al., 2006). These complex and multi-stage emplacement mechanisms characterize and enhance the capacity of these lavas to inundate a wider area, increasing the related volcanic hazards.

5. Conclusions

From this study we draw the following conclusions:

1. The integration of IDE and CDE permits to delineate the thermo-rheological space in which crystallization acts under near-equilibrium (IDE) and disequilibrium (CDE) conditions for La Palma basanitic melt;
2. In CDE the degrees of disequilibrium related to the cooling rates applied affect the rheological evolution of the melt and its timescales, favoring different rheological response of the suspension in the experimental range investigated. In detail, with increasing cooling rateboth onset of crystallization and interruption of experiments (i.e., attainment of the rheological cut-off or viscous rupture) occur at progressively lower temperatures and shorter times;
3. Combining rheological data and field observations we propose that the mechanisms characterizing the emplacement styles of Tajogaite lavas and their timescales (channels-tubes formation in proximal zone and pāhoehoe-ʻaʻā transition in distal zone) are primarily controlled by the degree of cooling rate at which the lava is subjected.

Conflict of Interest

The authors declare no conflicts of interest relevant to this study.

Data Availability Statement

Raw data are available on Figshare (DOI: https://doi.org/10.6084/m9.figshare.20523222).

Acknowledgments

This paper is dedicated to the memory of Professor Heidy Mader. This research was financially supported by the projects (I) MIUR Grants to Roma Tre PhD School in Earth Sciences (XXXIV doctoral cycle), (II) Grant of Excellence Departments, MIUR-Italy (ARTICOLO 1, COMMI 314 - 337 LEGGE 232/2016), (III) VOLRISKMAC (MAC/3.5b/124;), (IV) VOLRISKMAC II (MAC2/3.5b/328), financed by the Program INTERREG V A Spain-Portugal MAC 2014–2020 of the European Commission; (V) Cumbre Vieja Emergencia, financed by the Science and Innovation Ministry, Spanish Government; (VI) TFassistance, financed by the Cabildo Insular de Tenerife and (VII) LPvolcano, financed by the Cabildo Insular de La Palma. LC received funding from the Swiss National Science Foundation (Grant 200021_184632). We are grateful to Helge Gonnermann and one anonymous reviewer for their helpful and thoughtful comments. Christian Huber is also acknowledged for the valuable editorial guidance.

References

Arzilli, F., Polacci, M., La Spina, G., Le Gall, N., Llewellin, E. W., Brooker, R. A., et al. (2022). Dendritic crystallization in hydrous basaltic magmas controls magma mobility within the Earth's crust. *Nature Communications*, *13*(1), 3354. https://doi.org/10.1038/s41467-022-30890-8

Calvari, S., & Pinkerton, H. (1999). Lava tube morphology on Etna and evidence for lava flow emplacement mechanisms. *Journal of Volcanology and Geothermal Research*, *90*(3–4), 263–280. https://doi.org/10.1016/s0377-0273(99)00024-4

Campagnola, S., Vona, A., Romano, C., & Giordano, G. (2016). Crystallization kinetics and rheology of leucite-bearing tephriphonolite magmas from the Colli Albani volcano (Italy). *Chemical Geology*, *424*, 12–29. https://doi.org/10.1016/j.chemgeo.2016.01.012

Carracedo, J. C., Troll, V. R., Day, J. M. D., Geiger, H., Junca, M. A., Soler, V., et al. (2022). The 2021 eruption of the Cumbre Vieja volcanic ridge on La Palma. *Canary Islands*, *38*, 37. https://doi.org/10.1111/gto.12388

Cashman, K., Pinkerton, H., & Stephenson, J. (1999). Introduction to special section: Long lava flows. *Journal of Geophysical Research*, *103*(B11), 27281–27289. https://doi.org/10.1029/98jb01820

Cashman, K. V., Kerr, R. C., & Griffiths, R. W. (2006). A laboratory model of surface crust formation and disruption on lava flows through non-uniform channels. *Bulletin of Volcanology*, *68*(7–8), 753–770. https://doi.org/10.1007/s00445-005-0048-z

Chevrel, M. O., Cimarelli, C., de Biasi, L., Hanson, J. B., Lavallée, Y., Arzilli, F., & Dingwell, D. B. (2015). Viscosity measurements of crystallizing andesite from Tungurahua volcano (Ecuador). *Geochemistry, Geophysics, Geosystems*, *16*(3), 870–889. https://doi.org/10.1002/2014GC005661

Civico, R., Ricci, T., Scarlato, P., Taddeucci, J., Andronico, D., Bello, E., et al. (2022). *High-resolution digital surface model of the 2021 eruption deposit of Cumbre Vieja volcano* (pp. 1–7). La Palma. https://doi.org/10.1038/s41597-022-01551-8

Di Fiore, F., Mollo, S., Vona, A., MacDonald, A., Ubide, T., Nazzari, M., et al. (2021). Kinetic partitioning of major and trace cations between clinopyroxene and phonotephritic melt under convective stirring conditions: New insights into clinopyroxene sector zoning and concentric zoning. *Chemical Geology*, *584*, 120531. https://doi.org/10.1016/j.chemgeo.2021.120531

Di Fiore, F., Vona, A., Costa, A., Mollo, S., & Romano, C. (2022). Quantifying the influence of cooling and shear rate on the disequilibrium rheology of a trachybasaltic melt from Mt. Etna. *Earth and Planetary Science Letters*, *594*, 117725. https://doi.org/10.1016/j.epsl.2022.117725

Di Fiore, F., Vona, A., Kolzenburg, S., Mollo, S., & Romano, C. (2021). An extended rheological map of pāhoehoe—'A'ā transition. *Journal of Geophysical Research: Solid Earth*, *126*(7), 1–23. https://doi.org/10.1029/2021JB022035

Di Genova, D., Zandona, A., & Deubener, J. (2020). Unravelling the effect of nano-heterogeneity on the viscosity of silicate melts: Implications for glass manufacturing and volcanic eruptions. *Journal of Non-Crystalline Solids*, *545*, 120248. https://doi.org/10.1016/j.jnoncrysol.2020.120248

Giordano, D. (2019). Advances in the rheology of natural multiphase silicate melts: Importance for magma transport and lava flow emplacement. *Annales Geophysicae*, *62*, 1–24. https://doi.org/10.4401/ag-7859

Giordano, D., & Dingwell, D. B. (2003). Viscosity of Etna basalt: Implications for plinian-style basaltic eruptions. *Bulletin of Volcanology*, *65*(1), 8–14. https://doi.org/10.1007/s00445-002-0233-2

Giordano, D., Nichols, A. R. L., & Dingwell, D. B. (2005). Glass transition temperatures of natural hydrous melts: A relationship with shear viscosity and implications for the welding process. *Journal of Volcanology and Geothermal Research*, *142*(1–2), 105–118. https://doi.org/10.1016/j.jvolgeores.2004.10.015

Giordano, D., Polacci, M., Longo, A., Papale, P., Dingwell, D. B., Boschi, E., & Kasereka, M. (2007). Thermo-rheological magma control on the impact of highly fluid lava flows at Mt. Nyiragongo. *Geophysical Research Letters*, *34*(6), 2–5. https://doi.org/10.1029/2006GL028459

Giordano, D., Potuzak, M., Romano, C., Dingwell, D. B., & Nowak, M. (2008). Viscosity and glass transition temperature of hydrous melts in the system CaAl2Si2O8-CaMgSi2O6. *Chemical Geology*, *256*(3–4), 203–215. https://doi.org/10.1016/j.chemgeo.2008.06.027

González, P. J. (2022). Volcano-tectonic control of Cumbre Vieja. *Science*, *375*(6587), 1348–1349. https://doi.org/10.1126/science.abn5148

Gottsmann, J., Giordano, D., & Dingwell, D. B. (2002). Predicting shear viscosity during volcanic processes at the glass transition: A calorimetric calibration. *Earth and Planetary Science Letters*, *198*(3–4), 417–427. https://doi.org/10.1016/s0012-821x(02)00522-8

Harris, A. J. L., & Rowland, S. K. (2009). Effusion rate controls on lava flow length and the role of heat loss: A review. *Studies in volcanology: The legacy of George Walker* (Vol. 2, pp. 33–51). Special Publications of IAVCEI.

Ishibashi, H. (2009). Non-Newtonian behavior of plagioclase-bearing basaltic magma: Subliquidus viscosity measurement of the 1707 basalt of Fuji volcano, Japan. *Journal of Volcanology and Geothermal Research*, *181*(1–2), 78–88. https://doi.org/10.1016/j.jvolgeores.2009.01.004

Ishibashi, H., & Sato, H. (2007). Viscosity measurements of subliquidus magmas: Alkali olivine basalt from the Higashi-Matsuura district, Southwest Japan. *Journal of Volcanology and Geothermal Research*, *160*(3–4), 223–238. https://doi.org/10.1016/j.jvolgeores.2006.10.001

Jones, T. J., Le Moigne, Y., Russell, J. K., Williams-Jones, G., Giordano, D., & Dingwell, D. B. (2022). Inflated pyroclasts in proximal fallout deposits reveal abrupt transitions in eruption behaviour. *Nature Communications*, *13*(1), 2832. https://doi.org/10.1038/s41467-022-30501-6

Kempe, S. (2019). Volcanic rock caves. In *Encyclopedia of caves* (pp. 1118–1127). Academic Press.

Kolzenburg, S., Chevrel, M. O., & Dingwell, D. B. (2022). Magma/suspension rheology. *Reviews in Mineralogy and Geochemistry*, *87*(1), 639–720. https://doi.org/10.2138/rmg.2022.87.14

Kolzenburg, S., Di Genova, D., Giordano, D., Hess, K. U., & Dingwell, D. B. (2018). The effect of oxygen fugacity on the rheological evolution of crystallizing basaltic melts. *Earth and Planetary Science Letters*, *487*, 21–32. https://doi.org/10.1016/j.epsl.2018.01.023

Kolzenburg, S., Giordano, D., Cimarelli, C., & Dingwell, D. B. (2016). In situ thermal characterization of cooling/crystallizing lavas during rheology measurements and implications for lava flow emplacement. *Geochimica et Cosmochimica Acta*, *195*, 244–258. https://doi.org/10.1016/j.gca.2016.09.022

Kolzenburg, S., Giordano, D., Hess, K. U., & Dingwell, D. B. (2018). Shear rate-dependent disequilibrium rheology and dynamics of basalt solidification. *Geophysical Research Letters*, *45*(13), 6466–6475. https://doi.org/10.1029/2018GL077799

Kolzenburg, S., Hess, K., Berlo, K., & Dingwell, D. B. (2020). Disequilibrium rheology and crystallization kinetics of basalts and implications for the phlegrean volcanic district. *Frontiers of Earth Science*, *8*. https://doi.org/10.3389/feart.2020.00187

Kurokawa, A. K., Miwa, T., & Ishibashi, H. (2022). Aging in magma rheology. *Scientific Reports*, *12*, 1–7. https://doi.org/10.1038/s41598-022-14327-2

Longpré, M. A. (2021). Reactivation of Cumbre Vieja volcano. *Science*, *374*(6572), 1197–1198. https://doi.org/10.1126/science.abm9423

Mollo, S., & Hammer, J. E. (2017). Dynamic crystallization in magmas. *European Mineralogical Union Notes in Mineralogy*, *16*, 373–418. https://doi.org/10.1180/EMU-notes.16.12

Namiki, A., Lev, E., Birnbaum, J., & Baur, J. (2022). An experimental model of unconfined bubbly lava flows: Importance of localized bubble distribution. *Journal of Geophysical Research: Solid Earth*, *127*(6), e2022JB024139. https://doi.org/10.1029/2022jb024139

Oterino, B. B., Rejas, J. G., Murphy, P., Franco, R., Castro, D., Gacia-lanchares, C., & Sanchez, J. (2021). Temporal and spatial evolution of Cabeza de Vaca 2021 rift eruption (Cumbre Vieja volcano, La Palma, Canary Islands) from geophysical and geodesic paramethers analyses 1–35.

Pankhurst, M. J., Scarrow, J. H., Barbee, O. A., Hickey, J., Coldwell, B. C., Rollinson, G. K., et al. (2022). Rapid response petrology for the opening eruptive phase of the 2021 Cumbre Vieja eruption, La Palma, Canary Islands. *Volcanica*, *5*, 1–10. https://doi.org/10.30909/vol.05.01.0110

Sato, H. (2005). Viscosity measurement of subliquidus magmas: 1707 basalt of Fuji volcano. *Journal of Mineralogical and Petrological Sciences*, *100*(4), 133–142. https://doi.org/10.2465/jmps.100.133

Sauro, F., Pozzobon, R., Massironi, M., De Berardinis, P., Santagata, T., & De Waele, J. (2020). Lava tubes on Earth, Moon and Mars: A review on their size and morphology revealed by comparative planetology. *Earth-Science Reviews*, *209*, 103288. https://doi.org/10.1016/j.earscirev.2020.103288

Scarani, A., Vona, A., Di Genova, D., Al-Mukadam, R., Romano, C., & Deubener, J. (2022). Determination of cooling rates of glasses over four orders of magnitude. *Contributions to Mineralogy and Petrology*, *177*(3), 35. https://doi.org/10.1007/s00410-022-01899-5

Scarani, A., Zandonà, A., Di Fiore, F., Valdivia, P., Putra, R., Miyajima, N., et al. (2022). A chemical threshold controls nanocrystallization and degassing behaviour in basalt magmas. *Communications Earth & Environment*, *3*(1), 284. https://doi.org/10.1038/s43247-022-00615-2

Sehlke, A., Whittington, A., Robert, B., Harris, A., Gurioli, L., Médard, E., & Sehlke, A. (2014). Pahoehoe to áá transition of Hawaiian lavas: An experimental study. *Bulletin of Volcanology*, *76*(11), 876. https://doi.org/10.1007/s00445-014-0876-9

Soule, S. A., & Cashman, K. V. (2005). Shear rate dependence of the pāhoehoe-to-'a 'ā transition: Analog experiments. *Geology*, *33*(5), 361–364. https://doi.org/10.1130/G21269.1

Stevenson, R. J., Dingwell, D. B., Webb, S. L., & Bagdassarov, N. S. (1995). The equivalence of enthalpy and shear stress relaxation in rhyolitic obsidians and quantification of the liquid-glass transition in volcanic processes. *Journal of Volcanology and Geothermal Research*, *68*(4), 297–306. https://doi.org/10.1016/0377-0273(95)00015-1

Vetere, F., Murri, M., Alvaro, M., Domeneghetti, M. C., Rossi, S., Pisello, A., et al. (2019). Viscosity of pyroxenite melt and its evolution during cooling. *Journal of Geophysical Research: Planets*, *124*, 1451–1469. https://doi.org/10.1029/2018JE005851

Vona, A., Di Piazza, A., Nicotra, E., Romano, C., Viccaro, M., & Giordano, G. (2017). The complex rheology of megacryst-rich magmas: The case of the mugearitic "cicirara" lavas of Mt. Etna volcano. *Chemical Geology*, *458*, 48–67. https://doi.org/10.1016/j.chemgeo.2017.03.029

Vona, A., & Romano, C. (2013). The effects of undercooling and deformation rates on the crystallization kinetics of Stromboli and Etna basalts. *Contributions to Mineralogy and Petrology*, *166*(2), 491–509. https://doi.org/10.1007/s00410-013-0887-0

Vona, A., Romano, C., Dingwell, D. B., & Giordano, D. (2011). The rheology of crystal-bearing basaltic magmas from Stromboli and Etna. *Geochimica et Cosmochimica Acta*, *75*(11), 3214–3236. https://doi.org/10.1016/j.gca.2011.03.031

References From the Supporting Information

Arzilli, F., & Carroll, M. R. (2013). Crystallization kinetics of alkali feldspars in cooling and decompression-induced crystallization experiments in trachytic melt. *Contributions to Mineralogy and Petrology*, *166*(4), 1011–1027. https://doi.org/10.1007/s00410-013-0906-1

Bouhifd, M. A., Richet, P., Besson, P., Roskosz, M., & Ingrin, J. (2004). Redox state, microstructure and viscosity of a partially crystallized basalt melt. *Earth and Planetary Science Letters*, *218*(1), 31–44. https://doi.org/10.1016/s0012-821x(03)00641-1

Chevrel, M. O., Platz, T., Hauber, E., Baratoux, D., Lavallée, Y., & Dingwell, D. B. (2013). Lava flow rheology: A comparison of morphological and petrological methods. *Earth and Planetary Science Letters*, *384*(0), 109–120. https://doi.org/10.1016/j.epsl.2013.09.022

Giordano, D., Russell, J. K., & Dingwell, D. B. (2008). Viscosity of magmatic liquids: A model. *Earth and Planetary Science Letters*, *271*(1–4), 123–134. https://doi.org/10.1016/j.epsl.2008.03.038

Herschel, W. H., & Bulkley, R. (1926). Konsistenzmessungen von Gummi-Benzollösungen. *Kolloid Zeitschrift*, *39*(4), 291–300. https://doi.org/10.1007/BF01432034

Lanzafame, G., Mollo, S., Iezzi, G., Ferlito, C., & Ventura, G. (2013). Unraveling the solidification path of a pahoehoe "cicirara" lava from Mount Etna volcano. *Bulletin of Volcanology*, *75*(4), 1–16. https://doi.org/10.1007/s00445-013-0703-8

Llewellin, E., & Manga, M. (2005). Bubble suspension rheology and implications for conduit flow. *Journal of Volcanology and Geothermal Research*, *143*(1), 205–217. https://doi.org/10.1016/j.jvolgeores.2004.09.018

Scherer, G. W. (1984). Use of the Adam-Gibbs equation in the analysis of structural relaxation. *Journal of the American Ceramic Society*, *67*(7), 504–511. https://doi.org/10.1111/j.1151-2916.1984.tb19643.x

Whittington, A., Richet, P., & Holtz, F. (2000). Water and the viscosity of depolymerized aluminosilicate melts. *Geochimica et Cosmochimica Acta*, *64*(21), 3725–3736. https://doi.org/10.1016/s0016-7037(00)00448-8